Available online at www.sciencedirect.com

ScienceDirect

Geochimica et Cosmochimica Acta 304 (2021) 364–380

Geochimica et Cosmochimica Acta

www.elsevier.com/locate/gca

Potassium phases and isotopic composition in modern marine biogenic carbonates

Wenshuai Li [a], Xiao-Ming Liu [a,*], Kun Wang ("王昆") [b], F. Joel Fodrie [c], Toshihiro Yoshimura [d], Yong-Feng Hu [e]

[a] *Department of Geological Sciences, The University of North Carolina at Chapel Hill, Chapel Hill, NC 27599-3315, United States*
[b] *Department of Earth and Planetary Sciences and McDonnell Center for the Space Sciences, Washington University in St. Louis, MO 63130, United States*
[c] *Institute of Marine Sciences, The University of North Carolina at Chapel Hill, 3431 Arendell St., Morehead City, NC 28557, United States*
[d] *Japan Agency for Marine-Earth Science and Technology, 2-15, Natsushima-Cho, Yokosuka-city, Kanagawa 237-0061, Japan*
[e] *Canadian Light Source, The University of Saskatchewan, Saskatoon, SKS S7N 0X4, Canada*

Received 24 July 2020; accepted in revised form 9 April 2021; Available online 19 April 2021

Abstract

To investigate isotope fractionation between biogenic carbonates and modern seawater, we measured K concentration, phase, and isotopic composition in calcified skeletons from a variety of calcifying species. Samples included deep-sea corals, hermatypic corals, bivalves, gastropods, brachiopods, and planktonic foraminifera recovered globally over the past ten years in habitats with temperatures varying from 2 to 29 °C. The $\delta^{41}K$ values of the calcified organisms vary significantly, ranging from -0.72 ± 0.11 to 0.94 ± 0.04‰. Deep-sea corals exhibit the largest isotopic variability and the lowest $\delta^{41}K$, ranging from -0.72 ± 0.11 to 0.28 ± 0.09‰. Hermatypic corals display a moderate $\delta^{41}K$, ranging from -0.20 ± 0.07 to 0.37 ± 0.10‰. Bivalves display widely variable $\delta^{41}K$ values from 0.04 ± 0.05 to 0.94 ± 0.04‰, including the highest $\delta^{41}K$ observed. Gastropods exhibit $\delta^{41}K$ values between -0.42 ± 0.06 and -0.12 ± 0.06‰, while brachiopods have $\delta^{41}K$ values from -0.30 ± 0.05 to 0.24 ± 0.06‰. Limited foraminifera samples ($n = 2$) reveal $\delta^{41}K$ values of 0.15 ± 0.06 to 0.21 ± 0.06‰. Synchrotron-based atomic analyses show that K in biogenic carbonates is dominantly hosted in amorphous K_2CO_3, calcite-like and aragonite-like K phases, and intracrystalline organic matrices of varying proportions. The K isotopic composition of marine biogenic carbonates is not strongly temperature-dependent, in general, but correlates with skeletal K phases. This phase-control may indicate a first-order biological control on skeletal K incorporation, partitioning, and associated K isotope fractionation. This appears to reflect a substantial "vital effect"; i.e., physiological modification of the environmental information recorded in calcifying organisms. Substantial variations in $\delta^{41}K$ call for additional scrutiny before using marine biogenic carbonates to interpret ancient seawater $\delta^{41}K$ composition as physiological modulation substantially complicates the interpretation of marine carbonate $\delta^{41}K$ records through time. Future studies should include species-specific calibration with complementary synchrotron data to refine K isotope applications for paleoceanography.

Keywords: Calcification; Biomineralization; Seawater; Paleoceanography; Phase; X-ray absorption near-edge structure

* Corresponding author.
E-mail address: xiaomliu@unc.edu (X.-M. Liu).

https://doi.org/10.1016/j.gca.2021.04.018
0016-7037/

1. INTRODUCTION

Marine biogenic carbonate sediments and a variety of well-preserved calcified fossils are well-established as paleoclimate archives available for geochemical analysis of isotopes and trace elements (Jaffrés et al., 2007; Prokoph et al., 2008; Lough, 2010; Chen et al., 2018). Marine biogenic carbonates are pervasive geologic records and serve as valuable archives of seawater properties (Dellinger et al., 2018). Indeed the chemical composition of past seawater can be preserved in carbonate records and then recovered by multiple geochemical proxies (Rollion-Bard et al., 2019), including elemental ratios Li/Mg, B/Ca, Sr/Ca, Mg/Ca, U/Ca, and P/Ca, as well as isotopic compositions such as δ^{7}Li, δ^{11}B, δ^{44}Ca, δ^{53}Cr, δ^{98}Mo, $\delta^{238/235}$U, and ^{87}Sr/^{86}Sr (Ingalls et al., 2003; Weinstein et al., 2011; Noireaux et al., 2015; Frei et al., 2016; Bartlett et al., 2018; Dellinger et al., 2018; Marchitto et al., 2018; Füger et al., 2019). Carbonate sediments precipitate with different accretion rates ranging from centimeter to sub-millimeter scales per year (Henderson, 2002; Lough, 2010; Mitsuguchi and Kawakami, 2012; Rodriguez et al., 2014). Down-core analyses of biogenic carbonates have proven to be valuable for developing the proxies to reconstruct oceanographic histories across broad time scales from weeks to millions of years. These established proxies illuminated the usefulness of carbonate records with applications for tracing carbon and nutrient cycle, thermometry, weathering, and redox (Fodrie et al. 2017).

Advances in analytical methods using multiple collector-inductively coupled plasma-mass spectrometry (MC-ICP-MS) enable high-precision (better than 0.06‰) measurements of elemental isotopes (e.g., Li et al., 2016; Hu et al., 2018; Morgan et al., 2018; Chen et al., 2019; Xu et al., 2019; X. Li et al., 2020; Li and Han, 2021). Potassium (K) isotopes (^{41}K and ^{39}K, notated as δ^{41}K) have received increased attentions due to potentials for tracing low-temperature rock-fluid interaction and biogeochemical K cycling. Firstly, K is the sixth-most enriched metal in the Earth's crust and is enriched by orders of magnitude greater in silicates than carbonates. Therefore, seawater K isotopes are substantially affected by silicate weathering processes, including both continental and reverse weathering (e.g., S. Li et al., 2019; Santiago et al., 2020; Wang et al., 2020, 2021). Secondly, K is monovalent in nature and therefore exhibits no redox-related isotope fractionation. Thirdly, marked K isotope fractionation occurs during the formation of secondary silicate minerals and/or fluid-mineral exchange reactions (S. Li et al., 2019; Chen et al., 2020; Teng et al., 2020). Lastly, in hydroponic experiments, K isotopes seem to be substantially fractionated by land plants (Christensen et al., 2018). Uptake-driven isotope fractionation is expected due to its critical role as a macronutrient given K is one of the most abundant cations in plant cells, necessary for plant growth and development (Tripler et al., 2006; Sardans and Peñuelas, 2015). Thus, the riverine K budget may be dominated by biological utilization and silicate weathering. After continental runoff enters the ocean, seawater δ^{41}K values potentially reflect the processes modulating the carbon and K cycles on Earth's surfaces.

Since substantial K isotope fractionation occurs during (bio)geochemical weathering, the modern seawater δ^{41}K value (~0.14‰, Hille et al., 2019; Wang et al., 2020) is significantly higher than its major sources in the oceans (−1.0 to −0.6‰ and -0.38 ± 0.04‰, respectively for hydrothermal and river influxes, Zheng et al., 2019; Wang et al., 2021). Determining the evolution of the seawater K isotopic composition through time can help to understand the interplay between weathering, biosphere, and climate. Although there is little available research, past changes in the intensity and rate of (bio)geochemical weathering probably cause measurable variations in seawater δ^{41}K values. The usefulness of this novel proxy for paleoenvironmental applications requires comprehensive investigation. The K isotope composition of seawater may be recovered from K isotope analysis of marine carbonates. Nevertheless, a better understanding of whether and how marine carbonates record the K isotopic composition of seawater is necessary, including the basin-, temperature-, and species-specific dependence of seawater-carbonate K relationships. Furthermore, efforts to use marine carbonate δ^{41}K as an environmental proxy need to consider so-called "vital effects ", which potentially alter how information on seawater physiochemistry is recorded in biogenic calcified "hard parts" (Adkins et al.,2003; Saenger et al., 2013; Gothmann et al., 2016; Ullmann et al., 2017; Frei et al., 2018). Since K participates in biomineralization processes largely, there is a risk that abiotic or biotic factors fractionate K isotopes during K incorporation in biogenic precipitates as reported for other isotope and element proxies.

Here we report the K isotopic compositions in marine calcifying organisms (brachiopods, foraminifera, corals, gastropods, and bivalves) to assess whether biogenic carbonates reliably record the temporal K isotopic composition of precipitating seawater. This study links K phase partitioning with the K isotopic composition in marine biogenic carbonates from various geographic locations. Our objective is to investigate patterns and correlates of K incorporation and its isotope fractionation between marine carbonates and seawater to potentially apply K isotope system as a paleoenvironmental proxy.

2. MATERIALS AND ANALYSIS

2.1. Sample description

Biogenic carbonate samples in this study cover a wide range of taxonomic units, mineralogy (aragonite and low- and high-Mg calcite, Fig. S1), depositional environments (<10 m to near 2500 m in depth, including coastal zones to abyssal zones) and sampling locations (the Pacific Ocean and Atlantic Ocean, Fig. 1). Six broad taxa of marine biogenic carbonates (a total of 42 specimens) were investigated in this study:

(1) Deep-sea corals (*Corallium konojoi*, *Corallium konojoi*, *Paracorallium japonicum*, *and Corallium spp.*);
(2) Hermatypic corals (*Acropora sp.*, *and Porites sp.*);

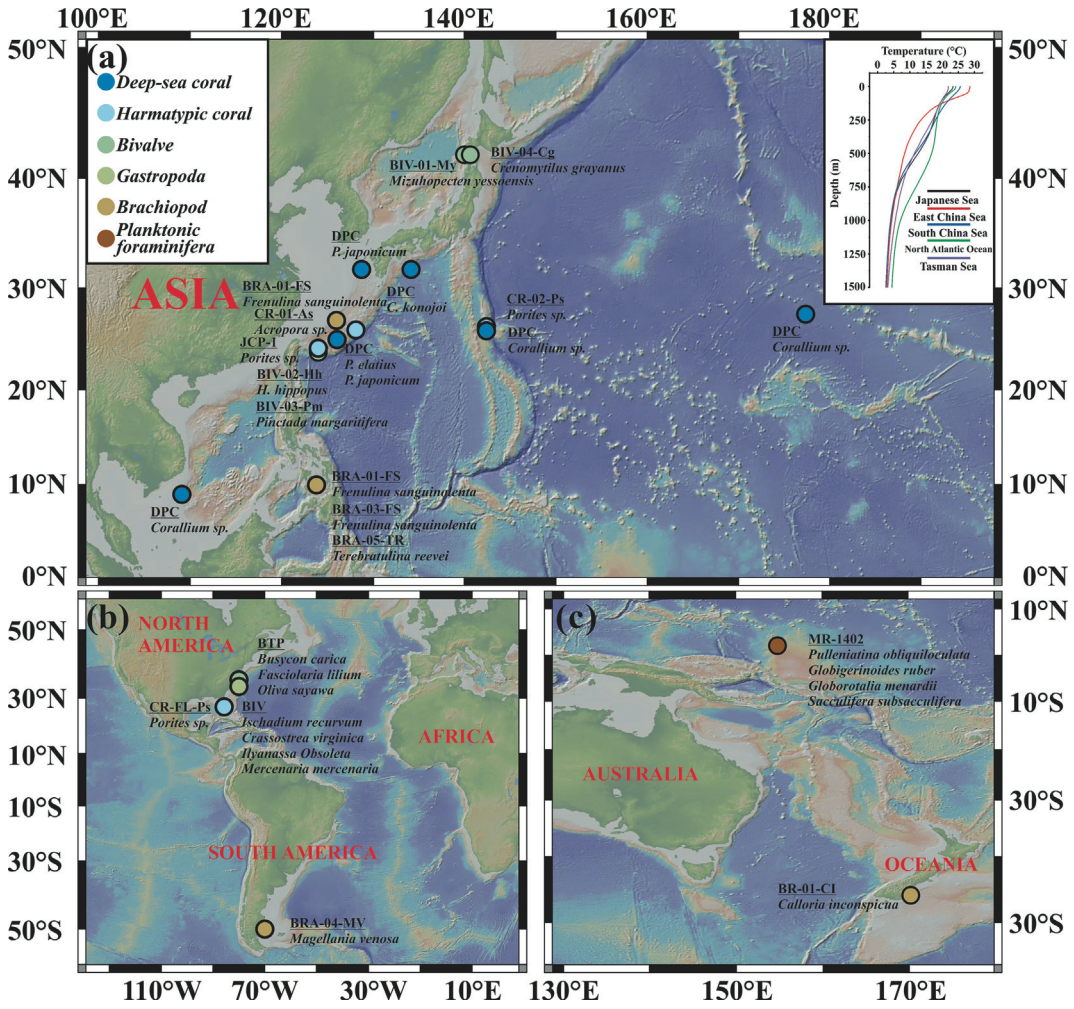

Fig. 1. Maps showing the sampling location and the name of specimens collected from (a) the North Pacific Ocean, (b) the Atlantic Ocean, and (c) the South Pacific Ocean. Inset bathymetric chart depicts the temperature sections (World Ocean Atlas 2013 Version 2).

(3) Bvalves (*Mizuhopecten yessoensis*, *Hippopus hippopus*, *Pinctada margaritifera*, *Crenomytilus grayanus*, *Ischadium recurvum, Crassostrea virginica*, *and Mercenaria mercenaria*);
(4) Gastropods (*Busycon carica*, *Fasciolaria lilium*, *and Oliva sayawa*);
(5) Brachiopods (*Calloria inconspicua*, *Terebratulina reevei, Frenulina sanguinolenta*, and *Magellaniavenosa sp.*);
(6) Planktonic foraminifera (*Pulleniatina obliquiloculata, Globigerinoides ruber, Globorotalia menardii*, and *Trilobatus sacculifer*).

Most coral samples have been investigated for C, O, Mg, S, and Na, which could be found in literature (Yoshimura et al., 2011; 2015a; 2015b; 2017). In addition to classical samples, planktonic foraminifera recovered from core-top sediments (0–8.5 cm below the seafloor) of the Ontong-Java Plateau (2450 m depth) were collected using a Piston Corer (Cruise MR14-02) and hand-picked under the binocular microscope. Brachiopods were sourced from Guido T. Poppe & Philippe Poppe, Conchology Inc. Gastropods and bivalves lived in intertidal environments to about 20 m depth. Detailed descriptions of the habitat of coral species should refer to Yoshimura et al. (2011). All the specimens were collected in the past ten years (Fig. 1). Mean annual water temperatures at the sampling localities ranged from 2.5 °C to 29.0 °C. Data were compiled from multi-station temperature data sourced from the Marine Science Institute, the University of North Carolina at Chapel Hill, and the Japan Oceanographic database http://ingrid.ldeo.columbia.edu/SOURCES/.LEVITUS94), respectively.

2.2. Sample location and features

It is known that deep-sea corals have a bathymetric distribution from several dozens to 2000 m depth. We collected a suite of deep-sea corals collected from the North and West Pacific oceans, in genera of *Corallium* and *Paracorallium* (Subclass Octocorallia, Order Alcyonacea, Family Coralliidae), having a dense, hard calcite skeleton (Yoshimura et al., 2011, Fig. 1). Deep-sea coral specimens were collected from a range of water depths of 30–1500 m, corresponding to a wide temperature range from

2.5 to 19.5 °C. Hermatypic corals (reef-building corals) are the major constituent of coral reefs formed in shallow (sub) tropical seawaters (normally less than 30 m depth). We collected massive (*Porites* sp., including an international coral standard JCp-1, Geological Survey of Japan) and branching (*Acropora sp.*) scleractinian corals from the North Pacific and Gulf of Mexico, which were composed of aragonite (Yoshimura et al., 2011). In addition, we sampled aragonite/calcite-mixed bivalves and gastropods from the Uchiura Bay (Hokkaido, Japan) and Back Sound (North Carolina, USA) (some were reported in Yoshimura et al., 2011, Fig. S1). We used planktonic foraminifera samples composed of high-Mg calcite skeleton from the Ontong-Java Plateau at the southwest Pacific (2450 m, Table S1). Brachiopods consisting of low-Mg calcite were collected from multiple places around the world during multiple expeditions, including the Southwest Pacific, Seragaki Dived (Japan), Golfo San Jose (Argentina), Punta Engano, Mactan Island, and Olango Island (Philippines) (Fig.S1).

2.3. Sample preparation

To ensure enough material for precise K isotope analysis, we collected ≥1 g bulk materials from each specimen. Carbonate samples were physically cleaned by sable brushes (Electron Microscopy Sciences, Fisher Scientific™) and a dental drill tool to remove animal tissues and obvious foreign materials. After that, the outermost material (~2 mm) was carefully removed from each sample using a microdrill to minimize potential surface contaminations. Samples were ultrasonicated with methanol and then rinsed with deionized water three times to remove remaining surface impurities. Samples were finely powdered in an agate mortar, treated with multiple rinsing cycles with deionized water (18.2 MΩ·cm, Millipore™) and ultrasonication. This step was repeated until residual solutions were clear and concentrations of dissolved cations (e.g., Fe, Mn, Mg, Al, Li, and K) were below the detection limits of the quadrupole Q-ICP-MS. The mortar and pestle were washed between samples using 2% HNO_3 solutions then with deionized water to prevent cross-contamination. After that, samples were treated with NH_4AC cleaning steps documented in Saenger and Wang (2014) that exchangeable surface complexes can be easily precluded with 1 M NH_4AC solutions followed by deionized water rinse in triplicate. For oxidative cleaning, all samples were subjected to two cycles of 5-min ultrasonication and rinsed with a mixed solution of 1:1 v/v 15% H_2O_2 and 0.5% $HClO_4$ (Cheng et al., 2000; Yoshimura et al., 2011). There are three types of organic materials: outer soft tissues, intercrystalline organic matrices, and intracrystalline organics. Despite of this effort, the first two could be eliminated, while the lattice-bounded intracrystalline organics could not be removed from the carbonate materials (Frei et al., 2018; Bruggmann et al., 2019).

Solid residues were rinsed using deionized water between each cleaning step to eliminate possible carry-over effects on K chemistry. Biogenic carbonate samples were recovered alive without identifiable Fe-Mn coatings, and thus, reductive cleaning was not necessary. Another concern is the potential impact on skeletal K/Ca ratio (and isotopic composition) by reductive cleaning, reported in an experimental study on foraminifera skeletal Mg/Ca (Barker et al., 2003). In the digestion step, 200–500 mg samples were weighed into 20 mL Teflon® beakers and dissolved in 0.05 M HCl + 30% H_2O_2 solutions in the thermostatic oven at 60 °C for over a week and transferred onto a hotplate over 120 °C until complete dissolution (W. Li et al., 2019). Released organic matrices from skeletons could be removed by chemical treatments using H_2O_2 to minimize interferences during Q-ICP-MS analysis.

To ensure that surface contaminations were negligible for bulk carbonate digestion, we tested bulk samples (after physical and oxidative cleaning steps) with synchrotron-based X-ray absorption spectroscopy. From K *K*-edge XANES data, non-carbonate K impurities can be avoided. To justify the effectiveness of our bulk digestion method for modern biogenic carbonates, we also performed a series of leaching experiments to determine the elemental and isotopic variations between leachates and bulk carbonates (Table S2). Two samples (a coral and a brachiopod after physical and oxidative cleaning) were investigated following commonly applied protocols for metal isotope systems (Table S2). The first approach included three individual leaching steps using 1 M acetic acid. This protocol successfully leached rare earth elements linked with calcite without affecting autogenic clays or Fe-Mn components (Cao et al. 2020). The second approach included three individual leaching steps with 0.2 M HCl under ambient conditions. In addition to carbonate phases, HCl treatment may also leach K from silicates and Fe-Mn coatings. The leaching procedures were modified from Pogge von Strandmann et al. (2019) and Clarkson et al. (2020). The acid leaching steps would help determine the influence of K contamination. Whenever possible, only leachates were analyzed for trace element ratios and K isotopic compositions (Figs. S2 and S3).

2.4. Analytical methods

Mineralogical and elemental characterizations were performed with an X-ray diffraction (XRD) and a Q-ICP-MS (Agilent™), respectively, at the University of North Carolina at Chapel Hill (Table S3). Dominant K phases in calcified skeleton were determined using K *K*-edge X-ray absorption near edge structure (XANES) acquired at the Soft X-ray Micro-Characterization beamline (SXRMB) of the Canadian Light Source (W. Li et al., 2020). K isotope analyses were performed using a MC-ICP-MS (Thermo Scientific™ Neptune Plus) at the Isotope Cosmochemistry Laboratory, Washington University in St. Louis. After separation, purified K-containing solutions (~3 μg) were introduced into the MC-ICP-MS. We used cold plasma to suppress the interferences from residual and isobaric ($^{40}Ar^1H^+$ on $^{41}K^+$ and $^{38}Ar^1H^+$ on $^{39}K^+$) argides (Chen et al., 2019). In addition to monitoring $^{41}K/^{39}K$ ratios, we measured $^{40}Ar/^{40}Ca$ ratios through ^{44}Ca to account for the interferences and contamination. Diluted K-bearing solutions of 5–8 mg·L^{-1} in 3% HNO_3 were introduced in the instrument by Elemental Scientific™ APEX omega,

equipped with a desolvation membrane to improve sensitivity and reduce hydride and oxide generation. Instrumental mass fractionation was corrected by a sample-standard bracketing method, and the sample-standard cycle was repeated with n sessions ($n \geq 5$). The instrumentation were given in Chen et al. (2019). The K isotopic compositions were reported in a δ-notation ($\delta^{41}K$), as parts per thousand (‰) deviation from the NIST SRM 3141a (Teng et al., 2017):

$$\delta^{41}K_{sample}(‰) = \left\{ \frac{(\,^{41}K/\,^{39}K)_{sample}}{(\,^{41}K/\,^{39}K)_{NIST\ SRM\ 3141a}} \right\} \times 1000 \quad (1)$$

Long-term reproducibility over a year was better than 0.11‰ based on repeated analyses of various international references (i.e., two standard deviation [S.D.] of mean across international reference measurements, Chen et al., 2019). Two USGS granodiorite (GSP-2) and basalt (BHVO-2) standards were measured, and $\delta^{41}K$ values fall into the uncertainty of reported data (Table S4), and good reproducibility of standards enables accurate isotope analysis. A GSJ coral standard JCp-1 (*Porites sp.*, −0.20 ± 0.07‰) and a USGS limestone NIST-SRM-1d (−0.20 ± 0.07‰) were also measured and reported for inter-laboratory comparison. The net isotope fractionation between components A and B ($\Delta^{41}K_{A\text{-}B}$) was defined as:

$$\Delta^{41}K_{A-B} = \delta^{41}K_A - \delta^{41}K_B \quad (2)$$

Confidential intervals (95% c.i.) were applied to reflect statistical clarity of data from each sample, calculated as (see also, Table 1):

$$95\%\text{c.i.}(‰) = t_{n-1} \times \frac{S.D.}{\sqrt{n}} \quad (3)$$

where S.D. is the standard deviation over analytical sessions (n times) of the sample, and t_{n-1} denotes student's law factor with (n − 1) degrees of freedom at a 95% confidence level. Estimated uncertainties on K isotopes were propagated based on the following equation:

$$\Delta E = \sqrt{(c_1\Delta W_1)^2 + (c_2\Delta W_2)^2 + \cdots + (c_n\Delta W_n)^2} \quad (4)$$

where ΔE is an absolute error, c is a multiplicative factor, and W is additive function inputs. Procedural blanks were monitored for experiment runs (≤10 ng K) and were found to be negligible in comparison to collected K fractions of standards and samples at μg- or mg-levels. Details of analytical method are given in the online supplementary information (SI).

3. RESULTS

3.1. Potassium and $\delta^{41}K$ in biogenic carbonates

Data rationality of presented element and isotope results can be confirmed based on the leaching experiments, and its justification is given in SI (“Evaluation of K contamination”). Skeletal K concentrations and element ratios are listed in Tables 1 and 2 and shown in Fig. 2a–b. Overall, substantial variations exist in skeletal K concentrations among different species of biogenic carbonates, following the descending order of hermatypic corals (139.6–317.1 μg/g), deep-sea corals (13.8–210.6 μg/g), gastropods (79.6–120.7 μg/g), bivalves (35.1–139.3 μg/g), brachiopods (29.9–106.7 μg/g), and planktonic foraminifera (36.0–68.6 μg/g). The K/Ca ratios in these samples span nearly two orders of magnitude, ranging from 0.05 to 2.23 mmol/mol. In particular, the variability in K/Ca ratios is large for deep-sea corals (0.06–2.38 mmol/mol) and brachiopods (0.10–1.08 mmol/mol). As for hermatypic corals, gastropods, bivalves, and planktonic foraminifera, K/Ca ratios range from 0.15 to 0.39, 0.18 to 0.36, 0.05 to 0.33, and 0.06 to 0.12 mmol/mol unit, respectively. We found no correlations between K/Rb, Al/Ca, Mn/Ca, P/Ca, and K/Ca ratios (Fig. S4).

The skeletal K isotopic compositions are summarized in Tables 1 and 2 and exhibited in Fig. 2c, together with the $\delta^{41}K$ composition of modern seawater and average upper continental crust (UCC) as documented in Hille et al. (2019) and Huang et al. (2020), respectively. The $\delta^{41}K$ values of marine biogenic carbonates varied greatly, ranging from -0.72 ± 0.11 to 0.94 ± 0.04‰. Specifically, skeletal K isotopic compositions range from -0.20 ± 0.07 to 0.37 ± 0.10‰ (hermatypic corals), -0.72 ± 0.11 to 0.28 ± 0.09‰ (deep-sea corals), 0.04 ± 0.05 to 0.94 ± 0.04‰ (bivalves), -0.42 ± 0.06 to -0.12 ± 0.06‰ (gastropods), -0.30 ± 0.05 to 0.24 ± 0.06‰ (brachiopods) and 0.15 ± 0.06 to 0.21 ± 0.06‰ (planktonic foraminifera). No apparent inter-species correlation was found between multiple elemental ratios indicative of contamination (K/Rb, Al/Ca, Mn/Ca, and P/Ca ratios) and sample $\delta^{41}K$ values (Fig. S5). There is no apparent correlation between temperature and skeletal K/Ca ratio among species (Fig. 3a). We found a negative logarithmic correlation ($R^2 = 0.21$) between skeletal K/Ca ratios (logarithmic) and K isotopic compositions among marine biogenic carbonates (Fig. 3b). A unified isotopic dependence on temperature was not observed (Fig. 3c), but $\delta^{41}K$ data of deep-sea coral *Corallium spp.* are negatively linked to temperature (Fig. 3d).

3.2. Potassium *K*-edge XANES of biogenic carbonates

The K *K*-edge XANES spectra and the first spectra derivatives of references and biogenic carbonates are shown in Figs. 4 and S6, and the XANES-LCF data are listed in Table 3.

We identified K in carbonate phases (amorphous K_2CO_3, calcite-like and aragonite-like K) and organic phases (soluble organic matrices OM-K1 and insoluble organic matrices OM-K2). The fraction of K_2CO_3 phase in marine biogenic carbonates ranges from $17.1 \pm 0.2\%$ to $28.8 \pm 0.2\%$ (hermatypic corals), $1.1 \pm 0.1\%$ to $7.7 \pm 0.3\%$ (deep-sea corals), $1.1 \pm 0.2\%$ to $23.6 \pm 0.7\%$ (bivalves), $9.3 \pm 0.3\%$ (a gastropod), $32.3 \pm 0.8\%$ (a brachiopod), and $9.8 \pm 0.3\%$ (a planktonic foraminifera). The proportion of K hosted in skeletal organic matrices (a sum of OM-K1 and OM-K2 phases) ranges from $22.4 \pm 0.3\%$ to $34.8 \pm 0.4\%$ (hermatypic corals), $34.5 \pm 0.3\%$ to $60.7 \pm 0.4\%$ (deep-sea corals), $20.0 \pm 0.4\%$ to $36.9 \pm 0.3\%$ (bivalves), $45.6 \pm 0.3\%$ (a gastropod), $38.8 \pm 0.2\%$

Table 1
Speciation, mineralogy and K chemistry of biogenic carbonates in this study.

Sample ID	Species	K (μg/g)	K/Ca (mmol/mol)	$\delta^{41}K$ (‰)	95% c.i. (‰)	$\Delta^{41}K$ (‰)	Depth (m)	Temp. (°C)	Mineralogy
Deep-sea coral									
DPC-1-23-T1	*Corallium konojoi*	61.7	0.19	0.24	0.06	0.20	100	19.5	Calcite
DPC-0812-B	*Corallium elatius*	48.6	0.17	0.13	0.09	0.23	250	18.0	Calcite
DPC-10	*Corallium elatius*	17.2	0.06	0.27	0.10	0.24	250	18.0	Calcite
DPC-11	*Paracorallium japonicum*	72.1	0.20	−0.25	0.05	0.19	100	19.5	Calcite
DPC-12	*Paracorallium japonicum*	82.1	0.19	0.28	0.09	0.23	100	19.5	Calcite
DPC-M6	*Paracorallium japonicum*	154.6	0.22	0.25	0.06	0.20	140	19.0	Calcite
DPC-K1	*Paracorallium japonicum*	114.6	1.22	−0.20	0.15	0.29	250	18.0	Calcite
DPC-K4	*Corallium spp.*	182.9	0.32	−0.72	0.11	0.25	100	19.5	Calcite
DPC-727	*Corallium spp.*	13.8	0.09	0.27	0.15	0.29	1500	2.5	Calcite
DPC-K3	*Corallium spp.*	48.3	0.23	0.21	0.06	0.20	700	6.5	Calcite
DPC-K5	*Corallium spp.*	171.7	0.22	−0.21	0.11	0.25	1000	3.5	Calcite
DPC-V1	*Corallium spp.*	190.6	0.28	−0.27	0.03	0.17	200–400	12.5	Calcite
DPC-V2	*Corallium spp.*	188.1	2.38	−0.51	0.15	0.29	200–400	12.5	Calcite
DPC-V3	*Corallium spp.*	117.7	0.20	−0.15	0.07	0.21	200–400	12.5	Calcite
DPC-V4	*Corallium spp.*	210.6	0.23	−0.34	0.08	0.22	200–400	12.5	Calcite
DPC-BIC	*Corallium spp.*	42.0	0.17	n.d.	n.d.	n.d.	200–400	12.5	Calcite
Hermatypic coral									
CR-01-As	*Acropora sp.*	139.6	0.15	0.31	0.06	0.20	<10	25.0	Aragonite
CR-02-Ps	*Porites sp.*	317.1	0.23	0.15	0.06	0.20	<10	24.5	Aragonite
CR-FL-Ps	*Porites sp.*	193.3	0.21	0.37	0.10	0.24	<10	25.0	Aragonite
JCp-1	*Porites sp.*	169.9	0.39	−0.20	0.07	0.21	<10	25.0	Aragonite
Bivalve									
BIV-01-My	*Mizuhopecten yessoensis*	37.4	0.05	0.11	0.08	0.22	n.d.	n.d.	Calcite
BIV-02-Hh	*Hippopus hippopus*	69.2	0.08	0.28	0.09	0.23	n.d.	n.d.	Aragonite
BIV-03-Pm	*Pinctada margaritifera*	35.1	0.06	0.94	0.04	0.18	n.d.	n.d.	Calcite
BIV-04-Cg	*Crenomytilus grayanus*	38.0	0.07	0.15	0.06	0.20	n.d.	n.d.	Aragonite
BIV-04-Hm1	*Ischadium recurvum*	120.8	0.20	0.12	0.07	0.21	<10	22.5	Aragonite
BIV-04-Hm2	*Ischadium recurvum*	116.3	0.24	0.36	0.10	0.24	<10	23.0	Aragonite
BIV-04-Eo	*Crassostrea virginica*	56.2	0.13	0.08	0.06	0.20	<10	24.0	Calcite
BIV-04-Ms	*Mercenaria mercenaria*	139.3	0.33	0.04	0.05	0.19	<10	23.0	Aragonite
BIV-04-Hc	*Mercenaria mercenaria*	63.4	0.20	0.25	0.12	0.26	<10	28.0	Aragonite
Gastropods									
BTP-04-KW	*Busycon carica*	79.6	0.20	−0.42	0.06	0.20	<10	23.0	Aragonite
BTP-04-BT	*Fasciolaria lilium*	86.1	0.18	−0.12	0.06	0.20	<10	23.0	Aragonite
BTP-04-LO	*Oliva sayawa*	120.7	0.36	−0.15	0.13	0.27	<10	22.5	Aragonite
Brachiopod									
BR-01-CI	*Calloria inconspicua*	29.9	0.10	0.06	0.05	0.19	n.d.	25.0	Calcite
BRA-01-FS	*Frenulina sanguinolenta*	48.9	1.08	0.24	0.06	0.20	25	29.0	Calcite
BRA-02-FS	*Frenulina sanguinolenta*	69.5	0.16	−0.01	0.05	0.19	30	25.0	Calcite
BRA-03-FS	*Frenulina sanguinolenta*	106.7	0.63	−0.18	0.13	0.27	100	27.0	Calcite
BRA-04-MV	*Magellania venosa*	32.3	0.13	−0.30	0.05	0.19	25	20.0	Calcite
BRA-05-TR	*Terebratulina reevei*	99.5	0.24	−0.30	0.05	0.19	400	10.0	Calcite
Planktonic foraminifera									
MR14-PL-01	*Pulleniatina obliquiloculata*	42.4	0.08	0.15	0.06	0.20	2450	23.3	Calcite
MR14-PL-02	*Globigerinoides ruber*	53.6	0.10	0.21	0.06	0.20	2450	27.4	Calcite
MR14-PL-03	*Globorotalia menardii*	36.0	0.06	n.d.	n.d.	n.d.	2450	20.7	Calcite
MR14-PL-04	*Trilobatus sacculifer*	68.55	0.12	n.d.	n.d.	n.d.	2450	26.0	Calcite

Note 1: "95% c.i." is the 95% confidence interval, representing two standard errors of five to seven analytical cycles corrected by the Student's *t* factor; See Hu et al. (2018) and Chen et al. (2019) for details.
Note 2: "Temp." is seawater temperature. "n.d." is "not determined". The calcification temperature of core-top foraminifera was calculated based on Mg/Ca thermometry (Anand et al., 2003; Mathien-Blard and Bassinot, 2009, Table S1).
Note 3: $\Delta^{41}K$ represents the K isotope fractionation between calcified skeletons and seawater (0.14‰, Hille et al., 2019; Wang et al., 2020), which can be calculated by subtracting the seawater $\delta^{41}K$ value from sample $\delta^{41}K$ values.

Table 2
Location, elemental ratios, and K partitioning coefficients of biogenic carbonates in this study.

Sample ID	Lat. / Log.	Bulk element analysis (after cleaning)							
		K/Ca (mmol/mol)	D_K	K/Rb (mol/mmol)	Al/Ca (mmol/mol)	Sr/Ca (mmol/mol)	Fe/Ca (mmol/mol)	Mn/Ca (μmol/mol)	P/Ca (mmol/mol)
Deep-sea coral									
DPC-1-23-T1	32°N / 134°′E	0.19	0.19	1.63	0.02	2.88	0.05	0.41	0.72
DPC-0812-B	25°N / 126°E	0.17	0.17	4.29	0.02	2.89	0.03	1.17	0.85
DPC-10	25°N / 126°E	0.06	0.06	1.45	0.01	2.98	0.07	1.28	1.00
DPC-11	32°N / 134°′E	0.20	0.20	2.15	0.08	3.14	0.03	0.35	0.85
DPC-12	32°N / 134°′E	0.19	0.19	5.71	0.03	2.67	0.02	0.53	0.63
DPC-M6	32°N / 128°E	0.22	0.22	3.58	0.03	2.78	0.03	0.84	0.53
DPC-K1	25°N / 126°E	1.22	1.23	0.45	0.07	2.93	0.02	0.91	0.64
DPC-K4	32°N / 132°E	0.32	0.33	1.02	0.01	2.99	0.04	0.97	0.62
DPC-727	27°N / 142°E	0.09	0.09	1.58	0.03	2.89	0.02	0.63	0.43
DPC-K3	27°N / 142°E	0.23	0.23	3.24	0.03	2.93	0.01	0.14	0.40
DPC-K5	28°N / 177°E	0.22	0.22	0.58	0.03	3.03	0.02	0.21	0.44
DPC-V1	9°N / 109°E	0.28	0.28	2.00	0.09	3.07	0.05	0.97	1.03
DPC-V2	9°N / 109°E	2.38	2.41	2.14	0.02	2.89	0.07	1.35	1.27
DPC-V3	9°N / 109°E	0.20	0.20	0.54	0.02	2.77	0.02	0.93	1.02
DPC-V4	9°N / 109°E	0.23	0.24	2.59	0.04	2.95	0.01	0.92	1.04
DPC-BIC	9°N / 109°E	0.17	0.17	0.25	0.01	3.13	0.05	1.02	0.43
Hermatypic coral									
CR-01-As	26°N / 127°E	0.15	0.15	3.25	0.09	9.76	0.05	0.99	0.06
CR-02-Ps	27°N / 142°E	0.23	0.23	2.56	0.07	10.39	0.02	0.54	0.01
CR-FL-Ps	28°N / 86°W	0.21	0.21	0.66	0.13	12.67	0.06	1.17	0.06
JCp-1	24°N / 124°E	0.49	0.49	2.43	0.15	8.76	0.06	1.55	0.04
Bivalve									
BIV-01-My	42°N / 140°E	0.05	0.05	1.25	0.06	1.28	0.03	0.45	0.04
BIV-02-Hh	24°N / 124°E	0.08	0.08	1.02	0.02	1.41	0.02	0.63	0.02
BIV-03-Pm	24°N / 124°E	0.06	0.06	2.63	0.04	1.25	0.02	0.83	0.08
BIV-04-Cg	42°N / 141°E	0.07	0.07	2.58	0.01	1.33	0.05	0.58	0.09
BIV-04-Hm1	32°N / 60°W	0.20	0.20	2.14	0.06	1.52	0.03	0.58	0.04
BIV-04-Hm2	32°N / 60°W	0.24	0.24	3.16	0.05	1.43	0.04	0.95	0.06
BIV-04-Eo	32°N / 60°W	0.13	0.13	1.87	0.04	1.06	0.04	0.68	0.07
BIV-04-Ms	32°N / 60°W	0.33	0.33	1.26	0.08	1.66	0.02	0.75	0.03
BIV-04-Hc	32°N / 60°W	0.20	0.20	2.36	0.04	1.72	0.02	0.85	0.05
Gastropod									
BTP-04-KW	32°N / 60°W	0.20	0.21	2.14	0.07	1.53	0.05	1.32	0.04
BTP-04-BT	32°N / 60°W	0.18	0.18	2.28	0.15	1.54	0.04	0.98	0.06
BTP-04-LO	32°N / 60°W	0.36	0.36	3.14	0.14	1.30	0.06	1.25	0.03
Brachiopod									
BR-01-CI	45°S / 171°E	0.10	0.10	2.28	0.04	1.19	0.06	0.91	0.55

BRA-01-FS	10°N / 124°E	1.08	1.09	3.65	0.05	1.18	0.07	1.34	0.05	
BRA-02-FS	28°N / 126°E	0.16	0.16	2.14	0.04	1.18	0.05	1.22	0.07	
BRA-03-FS	10°N / 124°E	0.63	0.63	1.58	0.02	1.24	0.04	1.57	0.13	
BRA-04-MV	45°S / 70°W	0.13	0.13	1.98	0.07	1.48	0.02	0.89	0.05	
BRA-05-TR	10°N / 24°E	0.24	0.24	2.36	0.07	1.52	0.03	1.28	0.34	
Planktonic foraminifera										
MR14-PL-01	2°N / 156°E	0.08	0.08	0.35	0.03	1.42	0.02	0.23	0.42	
MR14-PL-02	2°N / 156°E	0.10	0.11	0.45	0.05	1.49	0.02	0.16	0.66	
MR14-PL-03	2°N / 156°E	0.06	0.07	0.26	0.08	1.29	0.01	0.21	0.44	
MR14-PL-04	2°N / 156°E	0.12	0.12	0.85	0.05	1.36	0.02	0.11	0.53	

Note: D_K is the distribution coefficient of K between calcified skeletons and seawater, which can be calculated using the equation: $D_K = (K/Ca)_{Sample} / (K/Ca)_{Seawater}$ using molar ratios.

(a brachiopod), and $15.3 \pm 0.1\%$ (a planktonic foraminifera). The fraction of K-bearing calcite-like phase ranges from $31.3 \pm 0.1\%$ to $31.4 \pm 0.2\%$ (hermatypic corals), $30.0 \pm 0.1\%$ to $63.9 \pm 0.3\%$ (deep-sea corals), $51.8 \pm 0.1\%$ to $63.9 \pm 0.2\%$ (bivalves), $74.9 \pm 0.1\%$ (planktonic foraminifera), $45.1 \pm 0.2\%$ (gastropod) and $28.9 \pm 0.4\%$ (brachiopod). By contrast, K-bearing aragonite-like phase was only identified by XANES in hermatypic corals (33.8 ± 0.2 to $46.2 \pm 0.3\%$). We emphasize that the presence of calcite-like K phase, even in aragonitic species, does not necessarily refer to K preserved in calcite. Rather, it only reflects that its coordination environment is similar to that of K in abiotic calcite lattice.

4. DISCUSSION

4.1. Skeletal K speciation and incorporation

4.1.1. K incorporation in skeletal organic matrices

To understand the mechanism of K incorporation, we identify four major K phases using K *K*-edge XANES analyses for biogenic skeletons (Fig. 4), including amorphous K_2CO_3, calcite- and aragonite-like K phases, and K hosted in intracrystalline organic matrices. Our discovery is opposite to an early K *K*-edge XANES study of coral skeletons (*Porites lutea*, *P. lobata*, *Pavona gigantea*, and *Montastraea annularis*), which suggested that skeletal K neither substitutes for Ca in the aragonite nor presents within a discrete K_2CO_3 phase (Pingitore et al., 2001). Rather, Pingitore et al. (2001) speculated that K might complex with chlorine ion. The occurrence and distribution of K in biogenic carbonates emphasizes the importance of so-called "vital effects" - biologically mediated partitioning of K into organic matrices and/or carbonate phases. Skeletal organic mattrices cannot be fully excluded by oxidative cleaning, so the occurrence of K in intracrystalline organic matrices is expected considering K as one of macronutrient relevant to physiological and metabolic processes (Sinclair et al., 2006; Sardans and Peñuelas, 2015). The skeletal element/Ca analysis of corals and benthic foraminiferal species displays the rhythmic K enrichment where skeletal $CaCO_3$ crystals grow much fast with locally enriched organic materials (Allison and Finch, 2004; Meibom et al., 2008; Mitsuguchi and Kawakami, 2012). This feature could be ascribed to the formation of organic-K associations since organic matrices are enriched between $CaCO_3$ layers where calcification occurs (Janiszewska et al., 2011; Naumann et al., 2012). Hence, K could be enriched in skeletal organic matrices.

The incorporation of K into organic components as well as to carbonate phases is further supported by the distribution coefficient (D_K) describing K partitioning between seawater and carbonates during K removal from the calcification site, and D_K can be calculated as:

$$D_K = (K/Ca)_{Sample}/(K/Ca)_{Seawater} \quad (5)$$

Where (K/Ca) represents the molar ratio of K and Ca in calcified organisms and seawater. Our calculated D_K ranges from $0.05 \cdot 10^{-3}$ to $2.41 \cdot 10^{-3}$ with a median of $0.19 \cdot 10^{-3}$. The upper limit is characterized by a few exceptionally high

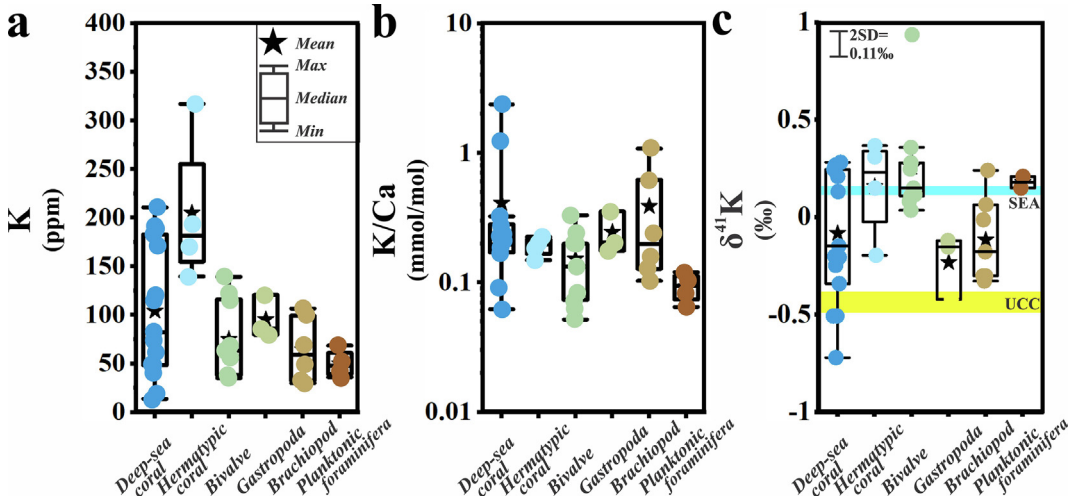

Fig. 2. Geochemical characterizations of modern biogenic carbonates, including (a) K concentration, (b) K/Ca ratio, and (c) K isotopic composition. Cyan and yellow bars in the box plots (c) represent the $\delta^{41}K$ signals of the upper continental crust (UCC, average $\delta^{41}K$ of $-0.44 \pm 0.05‰$, Huang et al., 2020) and the modern seawater (SEA, homogeneous $\delta^{41}K$ of about $0.14 \pm 0.02‰$, Hille et al., 2019; Wang et al., 2020), respectively. Long-term analytical uncertainty of K isotope analysis is 0.11‰ (2 S.D.) (external, Chen et al., 2019). In the x-axis, all data were arrayed in the sequence of deep-sea corals, hermatypic corals, bivalves, gastropods, brachiopods, and planktonic foraminifera from the left to right sides.

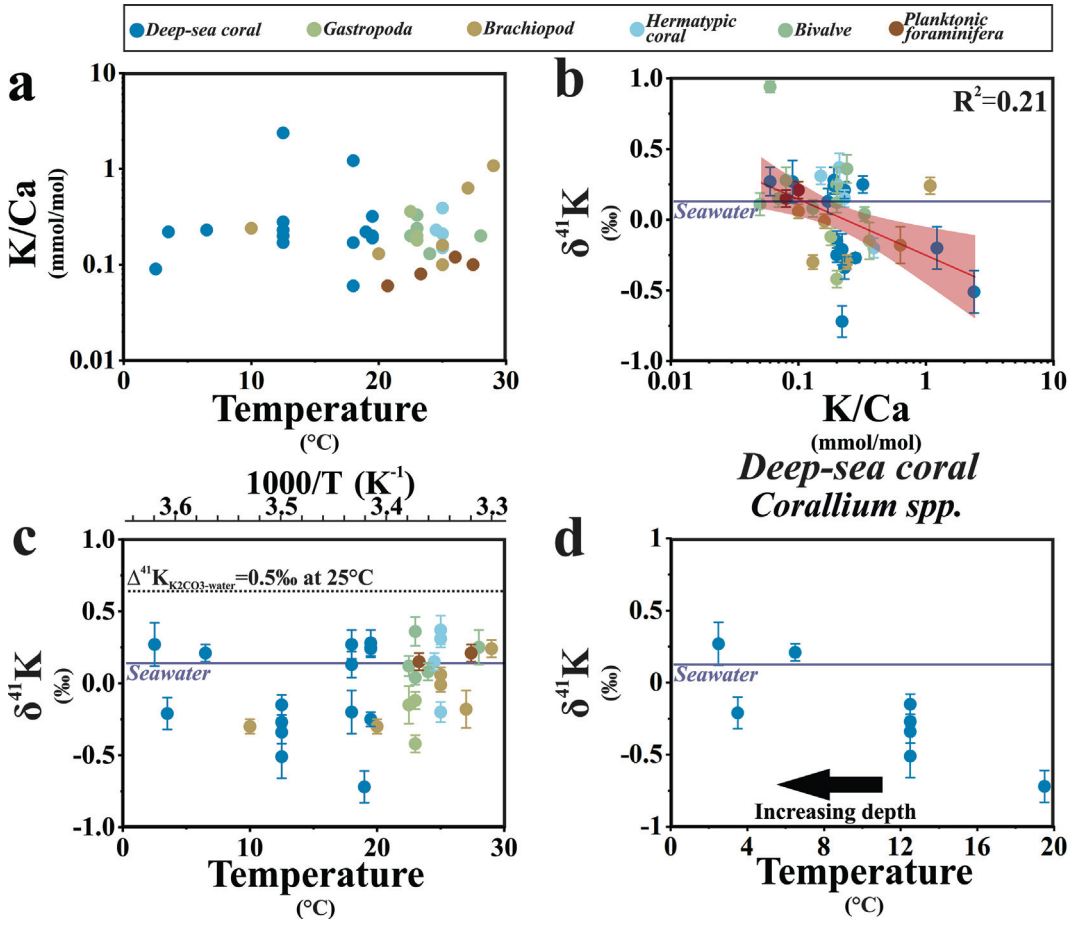

Fig. 3. Characterizing possible factors controlling K chemical compositions of biogenic carbonates. Interrelations of (a) temperature vs. skeletal K/Ca ratios; (b) K/Ca ratios vs. skeletal $\delta^{41}K$ values; and (c-d) temperature vs. skeletal $\delta^{41}K$ values. Skeletal $\delta^{41}K$ values of the deep-sea coral *Corallium spp.* collected from different depth across the temperature gradient are shown in the plot (d). The purple lines note the K isotopic composition of the modern seawater (~0.14‰, Hille et al., 2019; Wang et al., 2020), which is homogeneous globally. The black dotted line in the plot (c) highlights the equilibrium isotope fractionation of $K_2CO_3 \cdot 1.5H_2O$ from KCl solutions at 25 °C, theoretically provided in Li et al. (2017).

Table 3
Sample mineralogy and skeletal K phases determined based on XANES-LCF analysis.

Sample ID		XANES-LCF					
		K_2CO_3 (wt.%)	Soluble OM (wt.%)	Insoluble OM (wt.%)	Aragonite-like K (wt.%)	Calcite-like K (wt.%)	R
Deep-sea coral							
DPC-0812-B	*Corallium elatius*	4.6 (0.5)	36.8 (0.3)	15.8 (0.1)	0.0	42.8 (0.2)	0.002
DPC-11	*Paracorallium japonicum*	5.2 (0.2)	22.8 (0.6)	33.7 (0.2)	0.0	38.3 (0.1)	0.008
DPC-K1	*Paracorallium japonicum*	6.8 (0.1)	22.1 (0.2)	22.1 (0.2)	0.0	49.0 (0.2)	0.007
DPC-K5	*Corallium spp.*	6.8 (0.2)	15.5 (0.1)	19.0 (0.5)	0.0	58.7 (0.2)	0.005
DPC-V1	*Corallium spp.*	1.1 (0.1)	20.5 (0.4)	14.5 (1.1)	0.0	63.9 (0.3)	0.014
DPC-V3	*Corallium spp.*	7.7 (0.3)	28.4 (0.2)	33.9 (0.3)	0.0	30.0 (0.1)	0.012
DPC-V2	*Corallium spp.*	2.0 (0.3)	27.1 (0.2)	33.6 (0.3)	0.0	37.3 (0.5)	0.010
Hermatypic coral							
CR-01-As	*Acropora sp.*	0	17.1 (0.2)	5.3 (0.3)	46.2 (0.2)	31.3 (0.1)	0.001
CR-02-Ps	*Porites sp.*	0	28.8 (0.2)	6.0 (0.5)	33.8 (0.3)	31.4 (0.2)	0.002
Bivalve							
BIV-01-My	*Mizuhopecten yessoensis*	1.1 (0.2)	20.5 (0.2)	14.5 (0.3)	0.0	63.9 (0.2)	0.002
BIV-02-Hh	*Hippopus hippopus*	16.5 (0.3)	10.4 (0.1)	27.0 (0.3)	0.0	46.1 (0.5)	0.004
BIV-04-Eo	*Crassostrea virginica*	1.3 (0.2)	21 (0.5)	11.3 (0.3)	0.0	65.4 (0.4)	0.004
BIV-04-Hm1	*Ischadium recurvum*	13.2 (0.3)	11 (0.2)	23.8 (0.4)	0.0	51.8 (0.1)	0.002
BIV-04-Hm2	*Ischadium recurvum*	2.1 (0.3)	22.4 (0.2)	14.5 (0.4)	0.0	61.0 (0.3)	0.003
BIV-04-Ms	*Mercenaria mercenaria*	10.4 (0.2)	13.4 (0.1)	18.3 (0.6)	0.0	57.9 (0.4)	0.003
BIV-04-Hc	*Mercenaria mercenaria*	23.6 (0.7)	10 (0.3)	10.0 (0.5)	0.0	56.4 (0.3)	0.004
Gastropod							
BTP-04-KW	*Busycon carica*	9.3 (0.3)	17.3 (0.2)	28.3 (0.3)	0.0	45.1 (0.2)	0.003
Brachiopod							
BRA-02-FS	*Frenulina sanguinolenta*	32.3 (0.8)	0.0	38.8 (0.2)	0.0	28.9 (0.4)	0.005
Planktonic foraminifera							
MR14-PL-02	*Globigerinoides ruber*	9.8 (0.3)	0.0	15.3 (0.1)	0.0	74.9 (0.1)	0.004

Note 1: Molar contribution (%) of each K species to total K in carbonates as quantified by linear combination fitting (LCF) analysis of the first derivative of K *K*-edge XANES spectra of the best least square fit ranked after the R-factor (R).
Note 2: The standard errors in the parentheses are for the LCF analysis although the actual uncertainties for the overall XANES-LCF analysis could be lower. We note that the R-factor is a measure of goodness of fit.

D_K values ($(1.23–2.41) \cdot 10^{-3}$) from deep-sea corals *P. japonicum* and *Corallium spp.,* and a brachiopod *Frenulina sanguinolenta*. All D_K values are much less than 1 (i.e., broadly consistent with inorganic experiments, White, 1977; Ishikawa and Ichikuni, 1984; Okumura and Kitano, 1986), which could be explained by the difficulty of K^+ substitution of Ca^{2+} due to their valence and ionic radius differences. Most D_K values are higher than the D_K values of inorganically precipitated calcite ($\sim 0.5 \cdot 10^{-4}$ or lower) in $Ca(HCO_3)_2$-$MgCl_2$-KCl systems at 25 °C but lower than these of inorganically formed aragonite ($D_K \sim (0.5–0.9) \cdot 10^{-3}$) under the same condition (Okumura and Kitano, 1986). In $Ca(HCO_3)_2$-$MgCl_2$-NaCl-KCl systems (NaCl addition), the D_K values of inorganically crystalized aragonite dramatically decreased to $\sim 0.5 \cdot 10^{-4}$ because of Na^+ competition with K^+ for structural incorporation (Okumura and Kitano, 1986). Given above, the D_K values of marine biogenic carbonates are often higher than these of abiotic phases in seawater-like environments. We infer that intracrystalline organic matrices can promote K enrichment, resulting in higher K/Ca ratios relative to abiotically precipitated carbonates.

4.1.2. K incorporation in carbonates

In addition to K incorporation into organic components, we also evaluate how K can be incorporated in carbonate lattices since K in K_2CO_3 calcite-like and aragonite-like phases have been identified based on XANES-LCF results (Fig. 4). Carbonate growth is usually explained by an interfacial ion-by-ion addition theory (Nielsen et al., 2013). During precipitation, aqueous cations may be sequestered into carbonate structures through the propagation of skeletal materials and subsequent bond formation within the crystal. Here four possible mechanisms have been used to explain the partitioning of cations into carbonates based on previous literatures that may help to understand the case of K in this study (e.g., White, 1977; Ishikawa and Ichikuni, 1984; Okumura and Kitano, 1986; Mitsuguchi and Kawakami, 2012). Although existing studies lack direct evidence of the molecular host sites for K cations, we discuss these mechanisms as follows: (1) structural charge compensation by coupled substitution of K^+ with monovalent halide anions such as Cl^-; (2) K^+ incorporation for Ca^{2+} sites accompanied with structural defect forming; (3) altervalent substitution (structural ion replacement between ions with different valence states or anion vacancy) for Ca^{2+} sites; and (4) direct occupation at the interstitial space.

The K *K*-edge XANES spectra can help identify potential mechanisms of K incorporation. The absence of the XANES feature of KCl in biogenic carbonate (Figs. 4 and S6) excludes the first mechanism. As for the second mechanism, it was proposed that ion incorporation in carbonate lattice depends on the availability of structural defects and that defect density often positively correlates to carbonate precipitation rate (Teng et al., 2000; Dickinson et al., 2002; Yoshimura et al., 2017; Füger et al., 2019). Nevertheless, the growth rates of samples have not been constrained, and crystal defect quantification is also difficult. If the second mechanism plays a role, we would expect a general positive link between K/Ca ratios and trace element contents (e.g., Al, Mn, and P occupy the defects). However, we did not observe any significant correlations between skeletal K/Ca and trace element ratios from inter-species comparisons (Figs.S4). The lack of correlation maybe associated with the availability of crystal defects, which is limited. Therefore, structural defect forming is not likely the major mechanism driving K incorporation.

The last two mechanisms (i.e., K^+ altervalent substitution for Ca^{2+} and interstitial space occupation) are critical, both of which could potentially cause structural charge imbalance. The contribution from the last two mechanisms cannot be distinguished according to our results. Despite lacking direct K *K*-edge XANES evidence to examine the hypotheses, a reasonable assumption is that the last two processes correspond to the occurrence of K-bearing calcite-/aragonite-like phases (Fig. 4). The XANES-based calcite/aragonite-like K phases do not necessarily represent the K atoms hosted in calcite (orthorhombic crystal structure) or aragonite (trigonal-rhombohedral crystal structure). Rather, they likely reflect similar K coordination environments to these of chemically synthesized carbonates. Also, comparable atomic environments are the reason why calcite-like phases can be identified in aragonite corals. Previous studies propose that alkali metal ions (Li^+, Na^+ and K^+) prefer to substitute for nine-coordinated Ca^{2+} in aragonite while are prone to occupy structural defects and/or interstitial positions in abiotically precipitated calcite (Okumura and Kitano, 1986; Marriott et al., 2004a; Marriott et al., 2004b). The same distinct atomic environment may be true for K in calcifying organisms, causing spectral variations in K *K*-edge XANES.

4.2. Controls of the K isotope fractionation

4.2.1. Temperature dependence

The K isotope data indicate that marine biogenic carbonates are characterized by variable magnitudes of isotope fractionation, and there is no uniform temperature dependence of K isotope fractionation among species (Fig. 3c). This weak correlation is expected given a variety of species we analyzed (Table 1). We speculate that the influence of temperature on K isotope fractionation may be species-specific for calcifiers (i.e., isotope fractionation between calcified skeleton and surrounding seawater). For instance, we found a negative correlation between skeletal $\delta^{41}K$ value and temperature (deep-sea coral *Corallium spp.*), implying a species-specific temperature control (Fig. 3d). The temperature control reveals that biogeochemical K cycles and coordinated integration of coral tissues and skeletons respond to changes in temperature, which may be linked to metabolic modulation of the zooxanthellae and its coral host under thermal stress (Ferrier-Pagès et al., 2018). We conclude that the temperature sensitivity of $\Delta^{41}K$ in calcifying organisms is potentially species-specific. These *Corallium spp*. corals were collected from a range of water depths of 30–1500 m in the field (corresponding to a tem-

perature range from 2.5 to 19.5 °C), and the temperature impacts cannot be isolated from other potential factors such as pH and $[CO_3^{2-}]$. In sum, interspecific $\delta^{41}K$ variations are affected by environment variables, and may be directly induced by biomineralization processes as explained below.

4.2.2. A perspective of phase controls

Biologically mediated ion partitioning into a variety of skeletal ion phases have often been ignored in geochemical research. For example, zooxanthellate coral calcification is linked to the mutualistic relationships between coral polyp and endosymbiotic zooxanthellae (Warner et al., 1996). Hence, variations in the geochemical composition such as skeletal K isotope compositions are inevitably influenced by biological activities such as enzymatic photosynthetic reactions (Warner et al., 1996). Our K data provide another perspective that skeletal K isotope variability could be explained by K incorporation and its distribution within calcifying organisms. The comparison of skeletal K/Ca ratio versus $\delta^{41}K$ shows a general, negative correlation ($R^2 = 0.21$), implying mixing between two endmembers (Fig. 3b). We tentatively suggest an endmember (low K/Ca ratio and high $\delta^{41}K$) of carbonate phase because of preferential scavenging of ^{41}K in carbonates and limited K substitution for Ca from abiotic precipitation experiments (e.g., White, 1977; Ishikawa and Ichikuni 1984; Okumura and Kitano, 1986; Li et al., 2017). Another endmember (high K/Ca and low $\delta^{41}K$) may be the organic phases, as organic matrices enrich K relative to Ca (Mitsuguchi and Kawakami, 2012) and enrichments of light isotopes for organisms are observed (Wiederhold, 2015; Liu et al., 2019). This interpretation is supported by the plot of XANES-based phases versus $\delta^{41}K$ values (Fig. 5). Near-half of skeletal K is hosted in intracrystalline organic matrices in deep-sea corals, and most skeletal K is associated with carbonate phases for rest genera, particularly for foraminifera. Although collected K XANES data are limited and the mechanism of phase partitioning remains unknown, it is evident skeletal organic matrices play a sig-

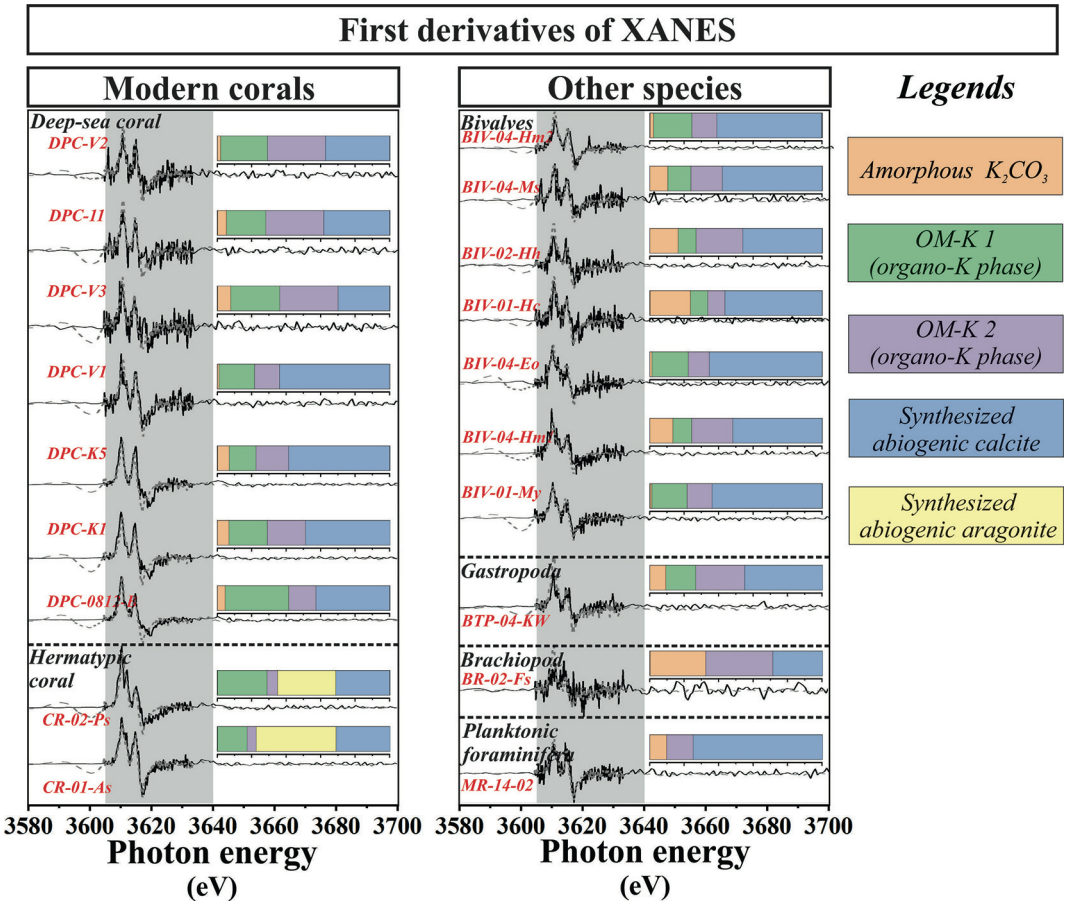

Fig. 4. The first derivatives of K *K*-edge XANES spectra of marine biogenic carbonates (deep-sea corals, hermatypic corals, bivalves, gastropods, brachiopods, and planktonic foraminifera). Each sample spectrum was averaged from triplicate analyses. The K-edge spectra were exhibited and treated with XANES-LCF analysis (using the Combo method, Manceau et al., 2012), based on different reference spectra displayed in Fig. 4 (X. Li et al., 2020; W. Li et al., 2020). Quantitative estimation for the proportion of each K-containing phase preserved in marine biogenic carbonates was present in the bar plot (a fitting range of 3605–3640 eV, grey regions). The XANES fitting data depend on the number, location, and magnitude of energy peaks. We note that K *K*-edge was detected with tender X-ray (1–5 keV) and the spectral noise reflects that skeletal K concentration is low and may limits the fitting result.

nificant role in K isotope fractionation. Considerable $\delta^{41}K$ variability in marine biogenic carbonates could be linked to the heterogeneous distribution of $\delta^{41}K$ signatures between different K components or phases coexisting in the skeletons. The dependence of $\delta^{41}K$ on skeletal phases can be ascribed to physiological modulation (K partitioning in organic matrices), and equilibrium processes (K hosted in carbonate lattices) dependent on the stiffness of structural K—O bonds, respectively. The two endmember contributions to skeletal $\delta^{41}K$ may be described by the equation: $\delta^{41}K_{Sample} = f_1 \times \delta^{41}K_{Organic} + f_2 \times \delta^{41}K_{Carbonate}$.

4.2.3. Isotope responses to carbonate phases

Given the presence of carbonate K phases by XANES (Fig. 4), we infer that the K isotope fractionation might occur due to the differences in properties of carbonate surfaces and bonding/coordination environments in carbonate structure. Here, we propose a possible mechanism - K structural incorporation via calcification processes, potentially causing K isotope fractionation following an equilibrium (thermodynamic) path associated with the bond stiffness (Schauble, 2004). We found the presence of K in K_2CO_3, calcite-like, and aragonite-like K phases according to K XANES data (Table 3). The incorporation of K into carbonate phases potentially results in equilibrium isotope fractionation of K along with altervalent K substitution for lattice Ca sites. Alternatively, K^+ might be fixed into structural defects and/or interstitial spaces (Ishikawa and Ichikuni, 1984). Therefore, we consider that the presence of K_2CO_3 and calcite-like K phases is predicted to favor isotopically heavier K (Fig. 5a), according to the equilibrium fractionation between $K_2CO_3{\cdot}1.5\ H_2O$(s) and precipitation fluids by theoretical estimation (Li et al., 2017, Fig. 3d). However, it is difficult to evaluate if individual K-bearing carbonate phases have distinct or near-consistent isotope compositions (e.g., calcite-K vs. aragonite K), but we suspect that isotopic compositions in different carbonate K phases likely vary. Using Li as an analog, an intra-shell δ^7Li variability (~25‰) in bivalve *Mytilus californianus* was found to be linearly correlated to the proportion of aragonite in skeletons (Dellinger et al., 2018). It reflects different δ^7Li compositions in carbonate minerals that are ascribed to different atomic environments of Li in aragonite and calcite (Okumura and Kitano, 1986). Similarly, different $\delta^{41}K$ signals in various carbonate phases are possible. We are cautious of over-interpreting this feature since mineralogy-dependence of $\delta^{41}K$ is not distinguished by XRD (Fig.S7), and other controls (e.g., physiological) may play a more important role. Future experimental work is required to test K isotope fractionation during carbonate precipitation.

4.2.4. Isotope responses to organic phases

The K isotopic composition in marine biogenic carbonates is impacted by the presence of organic substrate, based on the presence of OM-K phases in the "hard parts" of marine calcifiers (Fig. 4 and Table 3). Biological usage of K may induce K isotope fractionation, and the interference of K hosted within intracrystalline organic matrices cannot be eliminated solely by oxidative cleaning. Organic K phases can be identified using K *K*-edge XANES data, and there is an overall negative relationship between a sum of OM-K_{XANES} phases and $\delta^{41}K_{Sample}$ values (Fig. 5b). This relationship is expected as organisms preferentially take light K isotopes (Li et al., 2017). The isotope fractionation of K between calcified skeletons and seawater may be related to K closely involved in internal biological processes because K is the most abundant cellular cation used for physiological activities. Moreover, the morphology and nucleation of mineralizing carbonates are dictated by ion-transport proteins such as Na^+/K^+-ATPase (primary active transport), and there is strong biological modulation by the active transport of K for cellular processes (e.g., Boo et al., 2017; Galli and Solidoro, 2018; Ramesh et al., 2019). This interpretation can be further supported by the evidence that physiological activities modulate elemental partitioning and isotope fractionation between seawater and carbonates, or between $CaCO_3$ and intracrystalline organic matrices in calcified skeletons (Frei et al., 2018; Zhao et al., 2021). Biological control can be common in marine calcifying organisms. Although the $CaCO_3$ units for corals, foraminifera, bivalves, gastropods, and brachiopods form extracellularly in most cases, skeletal organic matrices are essential to modulate calcification by allowing crystallization (Von Euw et al., 2017) and which might sequester K. Therefore, biogenic carbonates are expected to prefer lighter K isotopes relative to their abiotic counterparts.

4.3. Implications for paleoceanography

Bulk carbonates have been used to trace past seawater compositions (e.g., Li: Sun et al., 2018; Mg: Saenger and Wang, 2014; U: Gilleaudeau et al., 2019). Sedimentary archives such as limestones are composed of bioclasts, which consist of bio-fragments from multi-taxonomy (or genera) calcified fossils of mollusks, corals, coccolithophores, brachiopods, algaes, and gastropods. This study provides a survey of K isotope fractionation between marine biogenic carbonates and contemporary seawater with applications for seawater chemistry reconstruction. Apparently, intra- and inter-species K isotopic compositions vary greatly and are at least partially associated with biological modulation. Therefore, K incorporation and distribution in various calcified archives need to be calibrated before the applications of stable K isotopes in paleoceanography. From another point of view, K isotopes likely provide a unique probe into the K speciation at the calcified sites. There is no unified temperature dependence of K isotope fractionation in studied marine samples. However, temperature control exists in an intra-species examination on deep-sea calcitic coral *Corallium spp.*, requiring further experimental constraints. Unfortunately, highly variable K/Ca ratios and $\delta^{41}K$ signals in marine biogenic carbonates complicate the utility of different taxa of widely used archives, such as hermatypic corals, deep-sea corals, bivalves, planktonic foraminifera, gastropods, and brachiopods. Furthermore, we infer that a similar issue may exist for calcified marine deposits in deep time, which could be ascribed to the partitioning of K in different phases. Although $\delta^{41}K$ data of foraminifera are limited ($n = 2$),

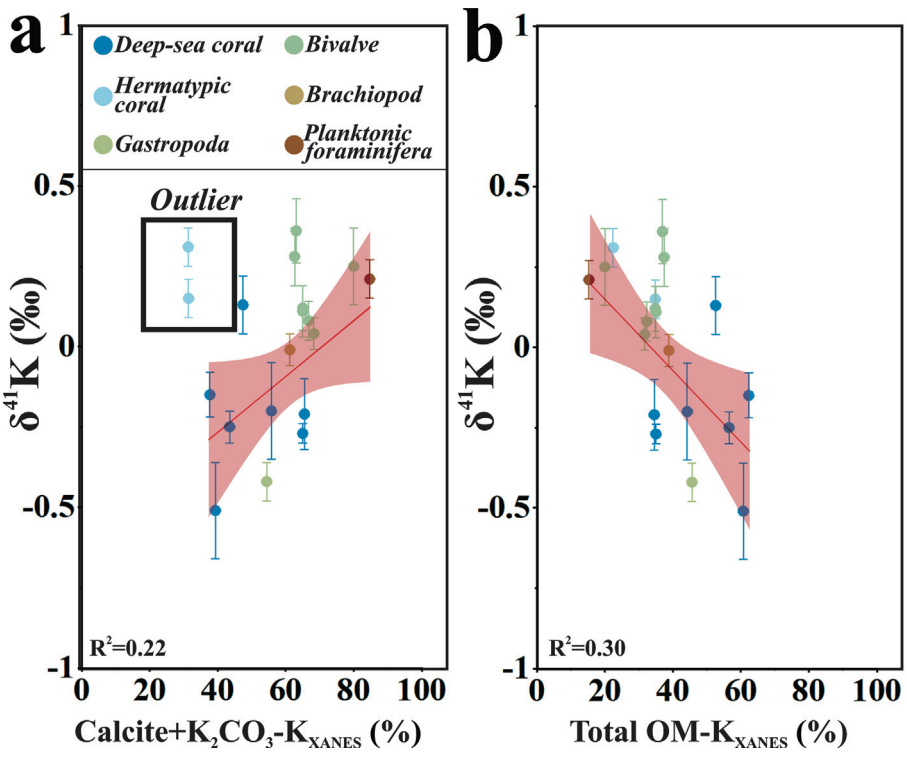

Fig. 5. Characterizing possible factors controlling the K chemical composition of deep-sea corals (*Corallium spp.*). Interrelation of (a) (calcite + K_2CO_3)-K_{XANES} vs. $\delta^{41}K$ values; (b) total OM-K_{XANES} vs. $\delta^{41}K$ values. Synchrotron-based identification of calcite-K_{XANES} phase (Table 3) is reasoned by K atoms hosted in carbonate lattices, situating in the coordination environment comparable to the coordination environment in laboratory synthetized calcite. The (calcite + K_2CO_3)-K_{XANES} is a sum of two different K phases preserved in calcite-like and K_2CO_3-like environments, and the total OM-K_{XANES} is a sum of two different K phases preserved in soluble and insoluble intracrystalline organic matrices (OM-K1 and OM-K2 in Fig. 4). Scleractinian coral K data are deviated from an overall positive trend in the plot (a), "marked as outliers". The data of these biogenic carbonates show strong dependence of K isotopic compositions on seawater temperature. Error bars in the x-axis are smaller than the symbol size and error bars in the y-axis show the 95% c.i. uncertainty. The red line shows linear fitting relationships, and the red area denotes 95% confidence.

their isotopic patterns are promising in recording seawater K isotopic composition. A comprehensive study of foraminifera $\delta^{41}K$ is needed. The usefulness of synchrotron radiation for calibrating and reconstructing seawater chemistry needs further assessment, including the acquisition of K composition in fossil calcifiers compared with respective modern species. Current understandings of K isotopes in biogenic carbonates are their infancy, and further refinements are essential.

5. CONCLUSIONS

We measured the elemental and isotopic composition of K in marine biogenic carbonates collected globally, including hermatypic corals, deep-sea corals, bivalves, brachiopods, planktonic foraminifera, and gastropods. We further identified the K phases in carbonate skeletons by synchrotron-based techniques. Main conclusions are summarized as follows:

(1) High-precision $\delta^{41}K$ analyses of marine biogenic carbonates exhibit considerable variation, ranging from -0.72 ± 0.11 to 0.94 ± 0.04‰. The K isotope fractionation in marine carbonate samples could lead to either positive or negative offsets from modern seawater K isotopic composition (~0.14‰). The $\delta^{41}K$ in marine biogenic carbonates could be linked to biologically mediated processes, controlling K incorporation and distribution in phases.

(2) Major K phases in marine biogenic carbonates include the K hosted in amorphous K_2CO_3, calcite-/aragonite-like phases, and intracrystalline organic matrices. Skeletal K incorporation reflects a combination of altervalent substitution, interstitial occupation, and organic associations.

(3) The K isotopic compositions in marine biogenic carbonates positively correlate with carbonate-like K phase following the equilibrium isotope fractionation law, while they are negatively correlated with the fraction of physiologically regulated organic-K component. Hence, skeletal K host proportions vary between species, driving K isotopic composition of calcified archives as an interplay of equilibrium and physiologically mediated processes at different levels.

(4) Intra-species and inter-species K isotopic variations are significant according to surveyed marine biogenic carbonates, and phase-dependence K isotope fractionation has been identified. Limited taxa and numbers of marine biogenic carbonate samples are studied; therefore, more systematic species-specific calibrations for $\delta^{41}K$ proxy and well-constrained culturing experiments are needed for future paleoceanography research.

Declaration of Competing Interest

The authors declare that they have no known competing financial interests or personal relationships that could have appeared to influence the work reported in this paper.

ACKNOWLEDGEMENTS

We acknowledge funding support from an NSF Career Award (EAR-1848153) to X. M. Liu, and the Martin fellowship from the University of North Carolina at Chapel Hill to W. S. Li. K. Wang thanks the McDonnell Center for the Space Sciences for financial support. We thank C. Rollion-Bard for editorial handling, and insightful feedback from the editor and anonymous reviewers whose comments improved the manuscript. We thank X. Wang and M. Shakouri for their help with XANES analysis and fruitful discussion. The K *K*-edge XANES were collected at Canadian Light Source (CLS), with the approval of CLS Proposal Review Committee (No. 30G09959 and 32G10898). The CLS is supported by the Canada Foundation for Innovation, Natural Sciences and Engineering Research Council of Canada, University of Saskatchewan, Government of Saskatchewan, Western Economic Diversification Canada, National Research Council Canada, and Canadian Institutes of Health Research.

APPENDIX A. SUPPLEMENTARY MATERIAL

Supplementary data to this article can be found online at https://doi.org/10.1016/j.gca.2021.04.018.

REFERENCES

Adkins J. F., Boyle E. A., Curry W. B. and Lutringer A. (2003) Stable isotopes in deep-sea corals and a new mechanism for "vital effects.". *Geochim. Cosmochim. Acta* **67**, 1129–1143.

Allison N. and Finch A. A. (2004) High-resolution Sr/Ca records in modern Porites lobata corals: Effects of skeletal extension rate and architecture. *Geochem. Geophys. Geosys.* **5** (5), Q05001.

Anand P., Elderfield H. and Conte M. H. (2003) Calibration of Mg/Ca thermometry in planktonic foraminifera from a sediment trap time series. *Paleoceanography* **18**, 1050.

Bartlett R., Elrick M., Wheeley J. R., Polyak V., Desrochers A. and Asmerom Y. (2018) Abrupt global-ocean anoxia during the Late Ordovician–early Silurian detected using uranium isotopes of marine carbonates. *Proc. Natl. Acad. Sci. USA* **115**, 5896–5901.

Bruggmann S., Klaebe R. M., Paulukat C. and Frei R. (2019) Heterogeneity and incorporation of chromium isotopes in recent marine molluscs (Mytilus). *Geobiology* **17**(4), 417–435.

Barker S., Greaves M. and Elderfield H. (2003) A study of cleaning procedures used for foraminiferal Mg/Ca paleothermometry. *Geochem., Geophy. Geosys.* **4**(9), 8407.

Boo M. V., Hiong K. C., Choo C. Y., Cao-Pham A. H., Wong W. P., Chew S. F. and Ip Y. K. (2017) The inner mantle of the giant clam, Tridacna squamosa, expresses a basolateral Na^+/K^+-ATPase α-subunit, which displays light-dependent gene and protein expression along the shell-facing epithelium. *PLoS ONE* **12**(10) e018686.

Chen H., Liu X. M. and Wang K. (2020) Potassium isotope fractionation during chemical weathering of basalts. *Earth Planet. Sci. Lett.* **539** 116192.

Chen H., Tian Z., Tuller-Ross B., Korotev R. L. and Wang K. (2019) High-precision potassium isotopic analysis by MC-ICP-MS: An inter-laboratory comparison and refined K atomic weight. *J. Anal. At. Spectrom.* **34**, 160–171.

Chen X., Romaniello S. J., Herrmann A. D., Samankassou E. and Anbar A. D. (2018) Biological effects on uranium isotope fractionation ($^{238}U/^{235}U$) in primary biogenic carbonates. *Geochim. Cosmochim. Acta* **240**, 1–10.

Christensen J. N., Qin L., Brown S. T. and Depaolo D. J. (2018) Potassium and Calcium Isotopic Fractionation by Plants (Soybean [Glycine max], Rice [Oryza sativa], and Wheat [Triticum aestivum]). *ACS Earth Sp. Chem.* **2**, 745–752.

Cheng H., Adkins J., Edwards R. L. and Boyle E. A. (2000) U-Th dating of deep-sea corals. *Geochim. Cosmochim. Acta* **64**(14), 2401–2416.

Clarkson M. O., Müsing K., Andersen M. B. and Vance D. (2020) Examining pelagic carbonate-rich sediments as an archive for authigenic uranium and molybdenum isotopes using reductive cleaning and leaching experiments. *Chem. Geol.* **539** 119412.

Cao C., Liu X. M., Bataille C. P. and Liu C. (2020) What do Ce anomalies in marine carbonates really mean? A perspective from leaching experiments. *Chem. Geol.* **532** 119413.

Dellinger M., West A. J., Paris G., Adkins J. F., Pogge von Strandmann P. A. E., Ullmann C. V., Eagle R. A., Freitas P., Bagard M. L., Ries J. B., Corsetti F. A., Perez-Huerta A. and Kampf A. R. (2018) The Li isotope composition of marine biogenic carbonates: Patterns and mechanisms. *Geochim. Cosmochim. Acta* **236**, 315–335.

Dickinson S. R., Henderson G. E. and McGrath K. M. (2002) Controlling the kinetic versus thermodynamic crystallisation of calcium carbonate. *J. Cryst. Growth* **244**(3–4), 369–378.

Fodrie F. J., Rodriguez A. B., Gittman R. K., Grabowski J. H., Lindquist N. L., Peterson C. H., Piehler M. F. and Ridge J. T. (2017) Oyster reefs as carbon sources and sinks. *Proc. Royal Soc. B* **284**(1859), 20170891.

Frei R., Crowe S. A., Bau M., Polat A., Fowle D. A. and Døssing L. N. (2016) Oxidative elemental cycling under the low O2 Eoarchean atmosphere. *Sci. Rep.* **6**.

Frei R., Paulukat C., Bruggmann S. and Klaebe R. M. (2018) A systematic look at chromium isotopes in modern shells–implications for paleo-environmental reconstructions. *Biogeosciences* **15**(16), 4905–4922.

Füger A., Konrad F., Leis A., Dietzel M. and Mavromatis V. (2019) Effect of growth rate and pH on lithium incorporation in calcite. *Geochim. Cosmochim. Acta* **248**, 14–24.

Ferrier-Pagès C., Sauzéat L. and Balter V. (2018) Coral bleaching is linked to the capacity of the animal host to supply essential metals to the symbionts. *Glob. Change Biol.* **24**(7), 3145–3157.

Gothmann A. M., Bende M. L., Blättler C. L., Swart P. K., Giri S. J., Adkins J. F., Stolaeski J. and Higgins J. A. (2016) Calcium isotopes in scleractinian fossil corals since the Mesozoic: Implications for vital effects and biomineralization through time. *Earth Planet. Sci. Lett.* **444**, 205–214.

Gilleaudeau G. J., Romaniello S. J., Luo G., Kaufman A. J., Zhang F., Klaebe R. M., Kah L. C., Azmy K., Bartley J. K., Zheng W., Knoll A. H. and Anbar A. D. (2019) Uranium isotope evidence for limited euxinia in mid-Proterozoic oceans. *Earth Planet. Sci. Lett.* **521**, 150–157.

Galli G. and Solidoro C. (2018) ATP supply may contribute to light-enhanced calcification in corals more than abiotic mechanisms. *Front. Mar. Sci.* **5**, 68.

Henderson G. M. (2002) New oceanic proxies for paleoclimate. *Earth Planet. Sci. Lett.* **203**, 1–13.

Hille M., Hu Y., Huang T. Y. and Teng F. Z. (2019) Homogeneous and heavy potassium isotopic composition of global oceans. *Sci. Bull.* **64**, 1740–1742.

Hu Y., Chen X. Y., Xu Y. K. and Teng F. Z. (2018) High-precision analysis of potassium isotopes by HR-MC-ICPMS. *Chem. Geol.* **493**, 100–108.

Huang T. Y., Teng F. Z., Rudnick R. L., Chen X. Y., Hu Y., Liu Y. S. and Wu F. Y. (2020) Heterogeneous potassium isotopic composition of the upper continental crust. *Geochim. Cosmochim. Acta* **278**, 122–136.

Ingalls A. E., Lee C. and Druffel E. R. M. (2003) Preservation of organic matter in mound-forming coral skeletons. *Geochim. Cosmochim. Acta* **67**, 2827–2841.

Ishikawa M. and Ichikuni M. (1984) Uptake of sodium and potassium by calcite. *Chem. Geol.* **42**, 137–146.

Jaffrés J. B. D., Shields G. A. and Wallmann K. (2007) The oxygen isotope evolution of seawater: A critical review of a long-standing controversy and an improved geological water cycle model for the past 3.4 billion years. *Earth-Sci. Rev.* **83**, 83–122.

Janiszewska K., Stolarski J., Benzerara K., Meibom A., Mazur M., Kitahara M. V. and Cairns S. D. (2011) A unique skeletal microstructure of the deep-sea micrabaciid scleractinian corals. *J. Morphol.* **272**(2), 191–203.

Lough J. M. (2010) Climate records from corals. *Wiley Interdiscip. Rev. Clim. Chang.* **1**, 318–331.

Li S., Li W., Beard B. L., Raymo M. E., Wang X., Chen Y. and Chen J. (2019a) K isotopes as a tracer for continental weathering and geological K cycling. *Proc. Natl. Acad. Sci. USA* **116**, 8740–8745.

Li W., Beard B. L. and Li S. (2016) Precise measurement of stable potassium isotope ratios using a single focusing collision cell multi-collector ICP-MS. *J. Anal. At. Spectrom.* **31**, 1023–1029.

Li W., Kwon K. D., Li S. and Beard B. L. (2017) Potassium isotope fractionation between K-salts and saturated aqueous solutions at room temperature: Laboratory experiments and theoretical calculations. *Geochim. Cosmochim. Acta* **214**, 1–13.

Li X., Han G., Zhang Q. and Miao Z. (2020a) An optimal separation method for high-precision K isotope analysis by using MC-ICP-MS with a dummy bucket. *J. Anal. At. Spectrom.* **35**(7), 1330–1339.

Li X. and Han G. (2021) One-step chromatographic purification of K, Ca, and Sr from geological samples for high precision stable and radiogenic isotope analysis by MC-ICP-MS. *J. Anal. At. Spectrom.* **36**, 676–684.

Li W., Liu X. M. and Godfrey L. V. (2019b) Optimisation of lithium chromatography for isotopic analysis in geological reference materials by MC-ICP-MS. *Geostand. Geoanaly. Res.* **43**(2), 261–276.

Li W., Liu X. M. and Hu Y. F. (2020b) K and Ca *K*-edge XANES in chemical compounds and minerals: implications for geological phase identification. *Geostand. Geoanaly. Res.* **44**(4), 805–819.

Liu, K., Wu, L. and Schiff, S. L. (2019). Use of Multi-collector ICP-MS for Studying Biogeochemical Metal Cycling. In Analytical Geomicrobiology. Cambridge University Press.

Manceau A., Marcus M. A. and Grangeon S. (2012) Determination of Mn valence states in mixed-valent manganates by XANES spectroscopy. *Am. Mineral.* **97**(5–6), 2816–2827.

Marchitto T. M., Bryan S. P., Doss W., McCulloch M. T. and Montagna P. (2018) A simple biomineralization model to explain Li, Mg, and Sr incorporation into aragonitic foraminifera and corals. *Earth Planet. Sci. Lett.* **481**, 20–29.

Marriott C. S., Henderson G. M., Belshaw N. S. and Tudhope A. W. (2004a) Temperature dependence of δ^7Li, δ^{44}Ca and Li/Ca during growth of calcium carbonate. *Earth Planet. Sci. Lett.* **222**, 615–624.

Marriott C. S., Henderson G. M., Crompton R., Staubwasser M. and Shaw S. (2004b) Effect of mineralogy, salinity, and temperature on Li/Ca and Li isotope composition of calcium carbonate. *Chem. Geol.* **212**, 5–15.

Mitsuguchi T. and Kawakami T. (2012) Potassium and other minor elements in Porites corals: Implications for skeletal geochemistry and paleoenvironmental reconstruction. *Coral Reefs* **31**, 671–681.

Morgan L. E., Santiago Ramos D. P., Davidheiser-Kroll B., Faithfull J., Lloyd N. S., Ellam R. M. and Higgins J. A. (2018) High-precision 41K/39K measurements by MC-ICP-MS indicate terrestrial variability of: δ41K. *J. Anal. At. Spectrom.* **33**, 175–186.

Meibom A., Cuif J. P., Houlbreque F., Mostefaoui S., Dauphin Y., Meibom K. L. and Dunbar R. (2008) Compositional variations at ultra-structure length scales in coral skeleton. *Geochim. Cosmochim. Acta* **72**(6), 1555–1569.

Mathien-Blard E. and Bassinot F. (2009) Salinity bias on the foraminifera Mg/Ca thermometry: Correction procedure and implications for past ocean hydrographic reconstructions. *Geochem. Geophys. Geosys.* **10**(12), Q12011.

Noireaux J., Mavromatis V., Gaillardet J., Schott J., Montouillout V., Louvat P., Rollion-Bard C. and Neuville D. R. (2015) Crystallographic control on the boron isotope paleo-pH proxy. *Earth Planet. Sci. Lett.* **430**, 398–407.

Naumann M. S., Richter C., Mott C., El-Zibdah M., Manasrah R. and Wild C. (2012) Budget of coral-derived organic carbon in a fringing coral reef of the Gulf of Aqaba, Red Sea. *J. Mar. Syst.* **105**, 20–29.

Nielsen L. C., De Yoreo J. J. and DePaolo D. J. (2013) General model for calcite growth kinetics in the presence of impurity ions. *Geochim. Cosmochim. Acta* **115**, 100–114.

Okumura M. and Kitano Y. (1986) Coprecipitation of alkali metal ions with calcium carbonate. *Geochim. Cosmochim. Acta* **50**, 49–58.

Prokoph A., Shields G. A. and Veizer J. (2008) Compilation and time-series analysis of a marine carbonate δ^{18}O, δ^{13}C, ^{87}Sr/^{86}Sr and δ^{34}S database through Earth history. *Earth-Sci. Rev.* **87**, 113–133.

Pogge von Strandmann P. A., Schmidt D. N., Planavsky N. J., Wei G., Todd C. L. and Baumann K. H. (2019) Assessing bulk carbonates as archives for seawater Li isotope ratios. *Chem. Geol.* **530** 119338.

Pingitore N. E., Villalobos J., Cruz-Jimenez G. and Wellington G. M. (2001) Incorporation of potassium in scleractinian coral aragonite: preliminary X-ray absorption spectroscopy. *AGUSM* **2001**, V41B-04.

Ramesh K., Yarra T., Clark M. S., John U. and Melzne F. (2019) Expression of calcification-related ion transporters during blue mussel larval development. *Ecol. Evol.* **9**(12), 7157–7172.

Rodriguez A. B., Fodrie F. J., Ridge J. T., Lindquist N. L., Theuerkauf E. J., Coleman S. E., Grabowski J. H., Brodeur M. C., Gittam R. K., Keller D. A. and Kenworthy M. D. (2014) Oyster reefs can outpace sea-level rise. *Nat. Clim. Change* **4**(6), 493–497.

Rollion-Bard C., Garcia S. M., Burckel P., Angiolini L., Jurikova H., Tomašových A. and Henkel D. (2019) Assessing the biomineralization processes in the shell layers of modern brachiopods from oxygen isotopic composition and elemental ratios: Implications for their use as paleoenvironmental proxies. *Chem. Geol.* **524**, 49–66.

Saenger C. and Wang Z. (2014) Magnesium isotope fractionation in biogenic and abiogenic carbonates: Implications for paleoenvironmental proxies. *Quat. Sci. Rev.* **90**, 1–21.

Saenger C., Wang Z., Gaetani G., Cohen A. and Lough J. M. (2013) The influence of temperature and vital effects on magnesium isotope variability in Porites and Astrangia corals. *Chem. Geol.* **360–361**, 105–117.

Santiago Ramos D. P., Coogan L. A., Murphy J. G. and Higgins J. A. (2020) Low-temperature oceanic crust alteration and the isotopic budgets of potassium and magnesium in seawater. *Earth Planet. Sci. Lett.* **541**.

Sardans J. and Peñuelas J. (2015) Potassium: A neglected nutrient in global change. *Glob. Ecol. Biogeogr.* **24**, 261–275.

Sinclair D. J., Williams B. and Risk M. (2006) A biological origin for climate signals in corals - Trace element "vital effects" are ubiquitous in Scleractinian coral skeletons. *Geophys. Res. Lett.* **33**.

Schauble E. A. (2004) Applying stable isotope fractionation theory to new systems. *Rev. Mineral. Geochem.* **55**, 65–111.

Sun H., Xiao Y., Gao Y., Zhang G., Casey J. F. and Shen Y. (2018) Rapid enhancement of chemical weathering recorded by extremely light seawater lithium isotopes at the Permian-Triassic boundary. *Proc. Natl. Acad. Sci. USA* **115**, 3782–3787.

Teng F. Z., Hu Y., Ma J. L., Wei G. J. and Rudnick R. L. (2020) Potassium isotope fractionation during continental weathering and implications for global K isotopic balance. *Geochim. Cosmochim. Acta* **278**, 261–271.

Teng F. Z., Dauphas N. and Watkins J. M. (2017) Non-Traditional Stable Isotopes: Retrospective and Prospective. In *Non-Traditional Stable Isotopes*. Walter de Gruyter GmbH, pp. 1–26.

Tripler C. E., Kaushal S. S., Likens G. E. and Todd Walter M. (2006) Patterns in potassium dynamics in forest ecosystems. *Ecol. Lett.* **9**, 451–466.

Teng H. H., Dove P. M. and De Yoreo J. J. (2000) Kinetics of calcite growth: surface processes and relationships to macroscopic rate laws. *Geochim. Cosmochim. Acta* **64**(13), 2255–2266.

Ullmann C. V., Frei R., Korte C. and Lüter C. (2017) Element/Ca, C and O isotope ratios in modern brachiopods: Species-specific signals of biomineralization. *Chem. Geol.* **460**, 15–24.

Von Euw S., Zhang Q., Manichev V., Murali N., Gross J., Feldman L. C., Gustafsson T., Flach C., Mendelsohn R. and Falkowski P. G. (2017) Biological control of aragonite formation in stony corals. *Science* **356**, 933–938.

Weinstein C., Moynier F., Wang K., Paniello R., Foriel J., Catalano J. and Pichat S. (2011) Isotopic fractionation of Cu in plants. *Chem. Geol.* **286**, 266–271.

Wang K., Close H. G., Tuller-Ross B. and Chen H. (2020) Global Average Potassium Isotope Composition of Modern Seawater. *ACS Earth Space Chem.* **4**(7), 1010–1017.

Wang K., Peucker-Ehrenbrink B., Chen H., Lee H. and Hasenmueller E. A. (2021) Dissolved potassium isotopic composition of major world rivers. *Geochim. Cosmochim. Acta* **294**, 145–159.

White A. F. (1977) Sodium and potassium coprecipitation in aragonite. *Geochim. Cosmochim. Acta* **41**, 613–625.

Warner M. E., Fitt W. K. and Schmidt G. W. (1996) The effects of elevated temperature on the photosynthetic efficiency of zooxanthellae in hospite from four different species of reef coral: a novel approach. *Plant Cell Environ.* **19**(3), 291–299.

Wiederhold J. G. (2015) Metal stable isotope signatures as tracers in environmental geochemistry. *Environ. Sci. Tech.* **49**(5), 2606–2624.

Xu Y. K., Hu Y., Chen X. Y., Huang T. Y., Sletten R. S., Zhu D. and Teng F. Z. (2019) Potassium isotopic compositions of international geological reference materials. *Chem. Geol.* **513**, 101–107.

Yoshimura T., Tanimizu M., Inoue M., Suzuki A., Iwasaki N. and Kawahata H. (2011) Mg isotope fractionation in biogenic carbonates of deep-sea coral, benthic foraminifera, and hermatypic coral. *Anal. Bioanal. Chem.* **401**(9), 2755–2769.

Yoshimura T., Suzuki A. and Iwasaki N. (2015a) Mechanism of O and C isotope fractionation in magnesian calcite skeletons of *Octocorallia* corals and an implication on their calcification response to ocean acidification. *Biogeosci. Discuss.* **12**, 389–412.

Yoshimura T., Tamenori Y., Takahashi O., Nguyen L. T., Hasegawa H., Iwasaki N., Kuroyanagi A., Suzuki A. and Kawahata H. (2015b) Mg coordination in biogenic carbonates constrained by theoretical and experimental XANES. *Earth Planet. Sci. Lett.* **421**, 68–74.

Yoshimura T., Tamenori Y., Suzuki A., Kawahata H., Iwasaki N., Hasegawa H., Nguyen L. T., Kuroyanagi A., Yamazaki T., Kuroda J. and Ohkouchi N. (2017) Altervalent substitution of sodium for calcium in biogenic calcite and aragonite. *Geochim. Cosmochim. Acta* **202**, 21–38.

Zheng X. Y., Beard B. L., Neuman M., Fahnestock M. F., Bryce J. G. and Johnson C. (2019) Constraining stable K isotope mass balance of the global ocean and its implications for the modern and past silicate cycle [abstract EP33C-2361]. *Am. Geophys. Union Fall Meet.*

Zhao M., Tarhan L. G., Zhang Y., Hood A., Asael D., Reid R. P. and Planavsky N. J. (2021) Evaluation of shallow-water carbonates as a seawater zinc isotope archive. *Earth Planet. Sci. Lett.* **553** 116599.

Associate editor: Claire Rollion-Bard